Materials Science-Poland, 36(2), 2018, pp. 177-184
http://www.materialsscience.pwr.wroc.pl/
DOI: 10.1515/msp-2018-0010

DE GRUYTER OPEN

Growth, spectral, density functional theory (DFT) and Hirshfeld surface analysis on 4-aminopyridinium adipate monohydrate nonlinear optical single crystal

R. VASANTHAKUMARI[1], W. NIRMALA[2], R. SANTHAKUMARI[3,*], R. MEENAKSHI[4], A. SINTHIYA[5]

[1]Department of Physics, Government Arts College (Autonomous), Karur-639 005, Tamil Nadu, India
[2]Department of Physics, Government Arts College, Tiruchirappalli-620 022, Tamil Nadu, India
[3]Department of Physics, Government Arts College for Women (Autonomous), Pudukkottai-622 001, Tamil Nadu, India
[4]Department of Physics, Cauvery College for Women, Tiruchirappalli- 600 018,Tamil Nadu, India
[5]Department of Physics, Srimad Andavan Arts and Science College (Autonomous), Tiruchirappalli-620 005, Tamil Nadu, India

4-aminopyridinium adipate monohydrate (4APA) was grown by slow evaporation solution growth technique. The functional groups in the grown crystal were identified from FT-IR spectral evaluation. The optical properties together with transmittance of the grown crystal were obtained from UV-Vis spectroscopic study. The mechanical and thermal properties of the grown crystal were studied using Vickers microhardness and TGA/DTA analyses, respectively. Microhardness test revealed that 4-aminopyridinium adipate monohydrate crystal is a soft category material. The density functional method (DFT) was performed using B3LYP with the 6-311G (d,p) basis set. The electronic charge distribution, reactivity of the molecules and the molecular electrostatic potential (MEP) of the grown crystal were analyzed using the B3LYP method. The intermolecular interactions that exist in the crystal structure of the 4APA have also been investigated by Hirshfeld surface analysis. The nonlinear optical properties of the 4APA crystal were confirmed by Kurtz-Perry technique.

Keywords: *crystal growth; growth from solution; Hirshfeld; DFT; organic material; nonlinear optical material*

1. Introduction

Materials exhibiting large optical nonlinearity are of great interest for the applications such as frequency conversion, telecommunications, optical computing, optical information processing and optical disk data storage [1–3]. The common knowledge is that an optical material should have a large charge transfer and optical transparency as well as low dislocation density. In recent years, the search for organic single crystal for the application in telecommunications, frequency doubling and optoelectronics has increased considerably [4–8]. The development of new organic nonlinear optical materials is attractive because of their advantages over the inorganic nonlinear optical materials. Aminopyridine and carboxyl groups together form many nonlinear optical complexes. Hydrogen bond interactions that exist in pyridine are the most important in heterocyclic chemistry. Adipic acid forms crystalline adipate via hydrogen bonding. It is known that adipic acid, though not the best as an acceptor forming various stacking complexes with different aromatic molecules, can also be useful as an acidic ligand. 4-aminopyridinium adipate is one of such donor-acceptor molecular compounds wherein adipic acid gives one of its proton (H) to the 4-aminopyridine, and adipic acid is transformed to mono-ionized state. In general, adipic acid can exist in acid and adipate forms in neutral and ionized state, respectively. In the ionized state it forms a robust intramolecular hydrogen bond with other molecule and also 4-aminopyridine molecules can exist in neutral and protonated state. The structure of 4-aminopyridinium adipate (4APA) has already been predicted [9]. Similarly to the above studies,

*E-mail: santhasrinithi@yahoo.co.in

single crystals of 4-aminyridinium adipate monohydrate have been grown by slow evaporation technique. The crystals were investigated using FT-IR, UV-Vis, Vickers microhardness, TGA/DTA, DFT and Hirshfeld surface analyses.

2. Experimental

4APA salt was synthesized by taking high purity (AR) grade sample of 4-aminopyridine and adipic acid in 1:1 molar ratio and dissolving the constituents in acetone solvent. Tanaka et al. [10] proposed that the crystal behavior can be influenced by two factors: the heat of crystallization and the solvent for growth. Based on this suggestion, for choosing an appropriate solvent for the growth of 4APA crystal, solubility test was performed in different solvents such as distilled water, acetone and other organic solvents. Finally, it was found that the 4APA salt had higher solubility in acetone compared to that of demineralized water and other solvents, hence, acetone was used as a solvent in the growth process. In order to grow single crystal of 4APA, in accordance with the solubility data, saturated solution was prepared and it was continuously stirred about two hours to ensure homogeneous concentration and temperature throughout the volume of the solution. Then the solution was filtered using a high quality Whatman filter paper (No. 5) to remove the solid colloidal particles. To obtain large single crystals, the bottom seed growth technique was adopted. The prepared saturated solution was taken in a beaker and covered by a perforated cover for controlled evaporation and kept in an undisturbed condition. The seed crystals of 4APA were obtained through spontaneous nucleation. The supersaturated solution of 4APA was carefully taken in a glass beaker and kept at 30 °C in a constant temperature bath. The defect free seed crystal was dropped into the supersaturated solution and the solution was allowed to evaporate the solvent slowly into the atmosphere. After a typical period of 20 to 26 days, colorless and transparent 4APA crystals have been obtained. The size of the big one was $18 \times 6 \times 2$ mm^3. The photograph of the grown crystal is shown in Fig. 1.

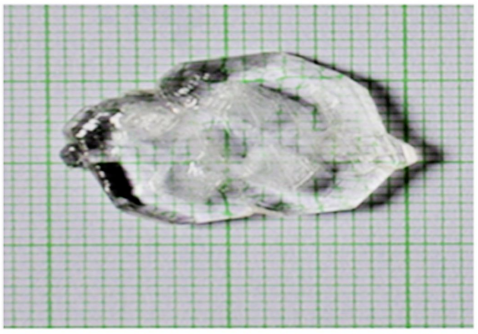

Fig. 1. As grown single crystal of 4APA.

3. Results and discussion

3.1. FT-IR spectral analysis

The recorded FT-IR spectrum for 4APA crystal is shown in Fig. 2. The observed vibrational frequencies have been confirmed qualitatively and their assignments are given in Table 1. The band at 3477 cm^{-1} is assigned to O–H stretching mode of vibration in IR spectrum. Medium bands discovered at 3318 cm^{-1} and 3229 cm^{-1}, respectively can be assigned to the NH_3^+ asymmetric stretching vibration mode [11]. The CH_3 symmetric deformation (isopropyl) is identified as the strong band at 1262 cm^{-1}. The protonated carboxyl group is generally identified by C–O stretching at 1700 cm^{-1} to 1780 cm^{-1}. The coordinations of amine and carboxylic compounds are confirmed by the presence of distinguished functional groups at 1704 cm^{-1} in the FT-IR spectrum [12].

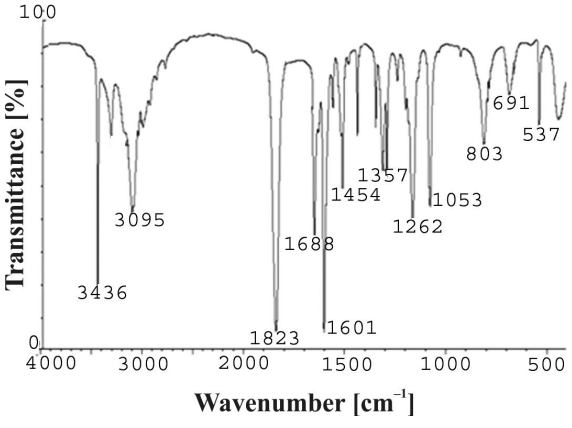

Fig. 2. FT-IR spectrum of 4APA crystal.

Table 1. FT-IR-spectral bands/peaks assignments for 4APA crystal.

Frequency [cm^{-1}]	Assignments
3456	O–H stretching vibration
3304 and 3095	NH_3^+ asymmetric stretching
1704	C–O carboxylic and carboxalate asymmetric stretching
1454	combination of C–C and O–H bending vibration
1357	COO^- symmetric stretching
1262	CH_3 symmetric stretching (isopropyl)
053	C–H in plane deformation mode
1012	O–H, C–H out of plane bending
803	CH_2 rocking vibration in phenyl ring
691	C–C stretching
537	NO_2 rocking

3.2. UV-Vis transmission study

The UV-Vis transmission spectrum of 4APA crystal was recorded with Perkin Elmer Lambda 35 spectrophotometer in the range of 200 nm to 1200 nm.The cutoff wavelength of 4APA crystal is 325 nm and its transmittance is above 58 % up to 1200 nm (Fig. 3).

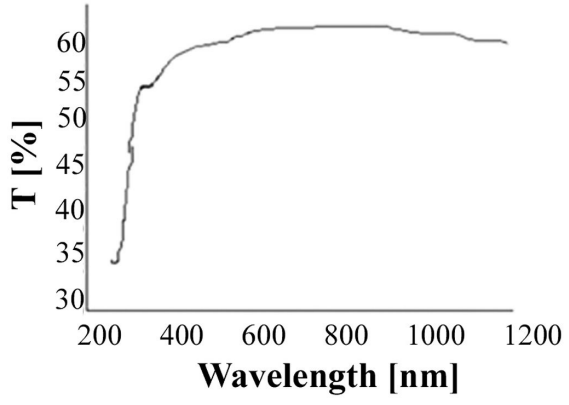

Fig. 3. UV-Vis spectrum of 4APA.

3.3. Microhardness study

Vickers's microhardness measurements were performed at room temperature. The Vickers microhardness number Hν was calculated using the relation:

$$H\nu = 1.8544(P/d^2)[\mathrm{kg/mm^2}] \qquad (1)$$

where P is the applied load (g) and d is the diagonal length (μm) of an indentation. The Hν values increase with increasing the load P. From the plot, it is revealed that the hardness number increases with an increase in load and it shows that the crystal exhibits reverse indentation size effect. The hardness increases gradually with the increase in the load up to 100 g, further increase in the load creates the cracks on the surface of the crystal due to the discharge of internal stresses produced by indentation [13]. Variation of load with Vickers hardness number (H_v) of 4APA crystal is shown in Fig. 4. The relation between the load and size of indentation is given by Mayer law:

$$P = ad^n \qquad (2)$$

where n is the work hardening coefficient or Mayer index, d is the recovered indentation in mm, a is a constant and P is the load [14]. The plot logP against logd is a straight line. The slope of the straight line gives the work hardening coefficient n. The work hardening coefficient for the grown crystal is found to be 3.75. Onitsch [15] pointed out that for hard materials n lies between 1 and 1.6 and for soft materials it is above 1.6. Based on the above statement, it is apparent that 4APA crystal belongs to soft material category.

3.4. Thermal analysis

The thermal balance of 4APA was studied with the aid of thermogravimetric analysis (TGA) and

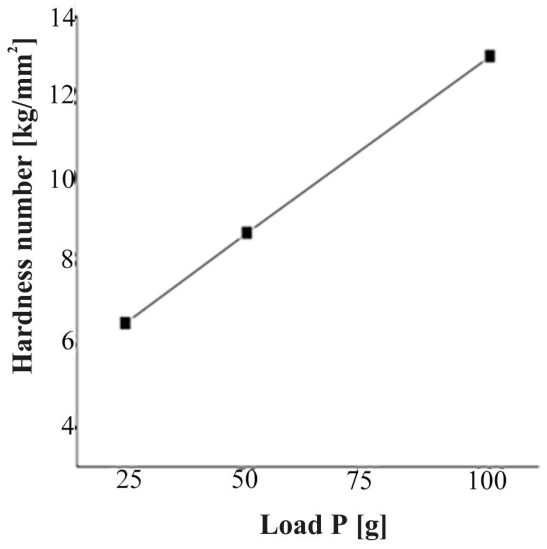

Fig. 4. Microhardness behavior of 4APA.

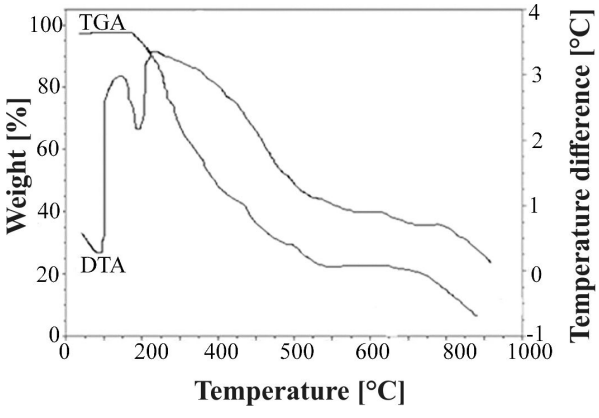

Fig. 5. TGA/DTA curve of 4APA.

differential thermal analysis (DTA) using SDT Q600 V8.3 Build 101 instrument between the temperatures of 50 °C and 1100 °C at a heating rate of 20 °C/min under nitrogen atmosphere (Fig. 5). The thermogravimetric analysis suggests that the material has very good thermal stability up to 200 °C. From the TGA curve it is seen that the decomposition of the title compound takes place in far interfered at a single stage weight loss. The endothermic peak at 200 °C in the DTA curve is assigned to the melting point of the title compound.

3.5. HOMO-LUMO analysis

The HOMO, LUMO analysis of the title molecule has been executed at B3LYP/6-311G level. The analysis of the wave function shows that, the electron absorption similar to the transition from the ground state to the first exited state can be described by means of one-electron excitation from the highest occupied molecular orbital (HOMO) to the lowest unoccupied molecular orbital (LUMO). The presence of orbital overlapping within the molecule reveals that there may be an intramolecular interaction between the bonding and antibonding molecular orbitals. Fig. 6 shows the mapped isodensity surface plots of molecular orbitals from HOMO − 3 to LUMO + 3 of the title molecule in which all the LUMO surfaces are well localized within the carboxypentanoate except LUMO + 3. In the assessment, all the mapped HOMO surfaces shown in Fig. 6 are well localized at the aminopyridinium group except HOMO − 3. The HOMO, LUMO energies of the title molecule, calculated at B3LYP/6-311G level, are collected in Table 2. The energy gap presented in Table 2 reflects the chemical activity of the molecule.

HOMO represents the potential to donate an electron and LUMO represents the ability to accept an electron. Among the subsequent excited states, the strongest transition appears between HOMO-LUMO orbitals. The numerical value of energy gap between HOMO-LUMO orbitals calculated at B3LYP level is −0.150839 a.u. The energy gaps for other possible energy transitions are also presented in Table 2.

3.6. Molecular electrostatic potential

Molecular electrostatic potential (MEP) at a point in the space around a molecule gives information about the net electrostatic effect produced at that point through total charge distribution (electron + proton) of the molecule [16]. Moreover, MEP surface helps to predict the reactivity of a wide variety of chemical systems in both electrophilic and nucleophilic reactions, the study of biological popularity strategies and hydrogen bonding interactions [17, 18]. Additionally it provides visible knowledge of relative

Table 2. The energy gaps for other possible energy transitions of 4APA.

Molecular orbitals	Energy E_H [a.u]	Molecular orbitals	Energy E_L [a.u]	Energy gap $\Delta E = E_L - E_H$ [a.u]
HOMO	−0.312004	LUMO	−0.161165	0.150839
HOMO − 1	−0.345666	LUMO + 1	−0.137827	0.208833
HOMO − 2	−0.351282	LUMO + 2	−0.105888	0.245402
HOMO − 3	−0.355006	LUMO + 3	−0.098284	0.256722

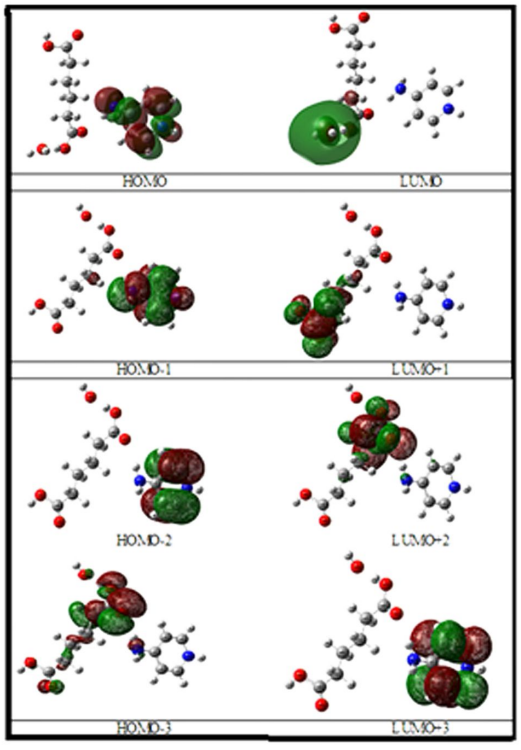

Fig. 6. Mapped isodensity surface plots of molecular orbitals of 4APA.

polarity of the molecule. An electron density isosurface mapped with electrostatic potential surface depicts the size, shape, charge density and reactive sites of the molecule. The different values of the electrostatic potential at the surface are represented by different colors; red represents regions of most electronegative electrostatic potential, blue represents regions of most positive electrostatic potential and green represents regions of zero potential. The electrostatic potential increases in the order red < orange < yellow < green < blue [19]. To predict reactive sites for electrophilic and nucleophilic attack in the investigated molecule, MEP surface is plotted over optimized geometry of 4APA at B3LYP/6-311G basis set. Fig. 7 shows electrostatic potential contour map with the electron density isosurface being 0.02 a.u. As easily can be seen in Fig. 7, the investigated molecule has possible sites for electrophilic (the electrophilic sites are most electronegative and are represented as red color) and nucleophilic attack (the nucleophilic sites are most positive and are represented as blue color). The fitting point charge to the electrostatic potential indicates that the atoms O19 and O21 are the most electronegative compared to O36 and O35. The uniform charge distributions on the ring addditives of aminopyridinium moiety protect the symmetry of the ring from substituent.

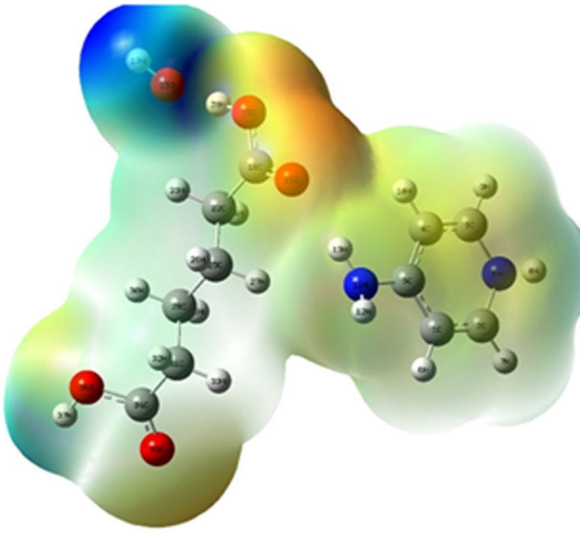

Fig. 7. Electrostatic potential contour map of 4APA.

3.7. NBO analysis

NBO analysis offers the maximally correct natural Lewis structure picture of ϕ, because the whole orbital information is mathematically

chosen to include the highest possible percentage of electron density. A beneficial issue of the NBO method is that it offers information about interactions in both filled and virtual orbital spaces that could enhance the analysis of intra- and intermolecular interactions. The second-order Fock matrix was used to assess the donor-acceptor interactions in NBO analysis [20]. The interactions result is the loss of occupancy from the localized NBO of the idealized Lewis structure into an empty non-Lewis orbital. For each donor (i) and acceptor (j), the stabilization energy:

$$E^{(2)} = \Delta E_{ij} = q_i \frac{F(i,j)^2}{\varepsilon_j - \varepsilon_i} \qquad (3)$$

where q_i is the donor orbital occupancy, ϵ_j and ϵ_i are diagonal elements and F(i,j) is the off diagonal NBO Fock matrix element. Natural bond orbital evaluation presents a green approach for studying intra- and inter-molecular bonding and interaction among bonds, and provides a convenient basis for investigating charge transfer or conjugative interaction in molecular systems. Some electron donor orbitals, acceptor orbitals and the interacting stabilization energy resulting from the second-order micro-disturbance theory are reported [20, 21]. The larger the Eð2Þ value, the more intensive is the interaction between electron donors and electron acceptors, i.e. the more donating tendency from electron donors to electron acceptors and the greater the extent of conjugation of the whole system. The DFT (B3LYP/6-311G) level computation is used to analyze the numerous second-order interactions between the filled orbitals of one subsystem and vacant orbitals of another subsystem, which is a measure of delocalization or hyper-conjugation [22].

NBOs are localized electron pair orbitals for bonding pairs and lone pairs. The hybridization of the atoms and the weight of each atom in each localized electron pair bond are calculated in the idealized Lewis structure. A regular Lewis structure does not leave any antibonding orbitals, so the presence of antibonding orbitals shows deviations from a normal Lewis structures. Antibonding localized orbitals are called non-Lewis NBOs. If the occupancy is not always 2.0, then there are deviations from an ideal Lewis structure. In order to study the small deviations from idealized Lewis structure, the donor-acceptor interaction approach is adopted. The calculated values of $E^{(2)}$ are shown in Table 3.

Table 3. The calculated values of $E^{(2)}$ of 4APA.

Donor (i)		Acceptor (j)		$E^{(2)}$	ϵ_i	ϵ_j
NBO	Type	NBO	Type	[kJ/mol]	[a.u]	[a.u]
π	C1-C2	n_1^*	C5	21.45	0.20	0.096
π	C3-C4	n_1^*	C5	23.39	0.20	0.099
n_1^*	C5	π^*	C1-C2	26.98	0.09	0.089
n_1^*	C5	π^*	C3-C4	25.55	0.09	0.089
n_1	N14	π^*	C1-C2	21.19	0.26	0.101

In the title compound, π(C3-C4)-n_1*(C5) interaction is seen to give a strong stabilization of 23.39 kJ/mol. This strong stabilization denotes the larger delocalization. The antibonding interactions are also involved in strong stabilization of molecule which are the interaction of n_1* with π*(C1-C2) and π*(C3-C4). These two interactions result in the stabilization energy of 26.98 and 25.55 kJ/mol, respectively. This highest interaction can produce the largest bioactivity inside the molecule.

3.8. Hirshfeld surface analysis

The quantitative intermolecular interaction has been studied using as a tool Hirshfeld surface analysis. Distribution of distances on packing surface of one molecule in an asymmetric unit and 2-D finger plot of the title compound are displayed in Fig. 8.

In the electrostatic potential, mapped on Hirshfeld surface with 0.24 a.u., the blue region corresponds to positive electrostatic potential and red region to negative electrostatic potential. The red vicinity represents the hydrogen bonding acceptor. The percentage of interaction is shown in Fig. 9.

The 2-D finger plot indicates that the intermolecular interaction is ruled by H–H interaction by occupying large area, whereas the O–H...O hydrogen bonding is identified via H–O interaction which is indicated by two wings in the Fig. 9. C–H interaction revealing the CH aromatic

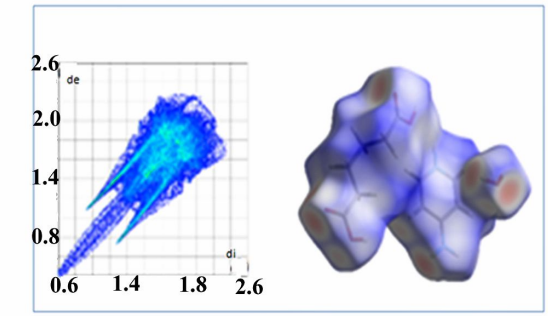

Fig. 8. 2D finger plot of 4APA.

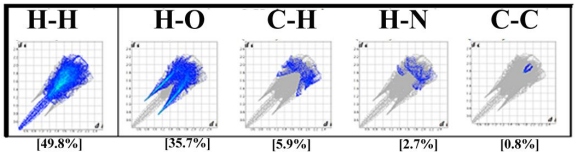

Fig. 9. The percentage of interaction.

molecules results in a symmetric pair of wings. And C–C interaction reveals the carboxylic group with 0.8 % interaction. The N–H interaction reveals the N–H...O hydrogen bonding.

3.9. Second harmonic generation

Kurtz et al. [23] second harmonic generation (SHG) test was performed on 4APA crystal in order to estimate the NLO efficiency. The powdered 4APA crystal with a uniform particle size was taken and packed in a microcapillary tube and was illuminated with a Spectra Physics Quanta Ray DHS2 Nd:YAG laser using the first harmonics output of 1064 nm with a pulse width of 8 ns and repetition rate of 10 Hz. A sample of potassium dihydrogen orthophosphate was used as a reference material in the present measurement. The input laser energy incident on the powdered sample was chosen to be 3.4 mJ. Powder SHG efficiency obtained for 4APA is about ∼3.0 times higher than that of potassium dihydrogen orthophosphate crystal.

4. Conclusions

4-aminopiridinium adipate monohydrate was grown at room temperature using slow evaporation technique. From the FT-IR study, the formation of the molecular structure of the material was confirmed. Optical transmittance window and the lower cut off wavelength were identified through UV-Vis-NIR. The microhardness test revealed mechanical strength of the material. Thermal analysis indicated that the crystal had good thermal stability. The electronic charge distribution and reactivity of the molecules within the crystal were studied by HOMO and LUMO analysis and the molecular electrostatic potential (MEP) of the grown crystal was also studied through B3LYP method. The intermolecular interactions that exist in the crystal structure were analyzed by Hirshfeld surface analysis. Second harmonic generation efficiency of the powdered 4APA crystal is ∼3.0 times higher than that of potassium dihydrogen orthophosphate.

Acknowledgements

Authors thank the CECRI, Karaikudi, for extending the lab facilities to record TGA/DTA. The authors acknowledge Prof. P.K. Das, Department of Inorganic and Physical Chemistry, Indian Institute of Science, Bangalore, for extending the laser facilities for SHG measurement.

References

[1] Ledoux I., *J. Synth. Met.*, 54 (1993), 137.
[2] Yuan D.R., Xu D., Zhang N., Liu M.G., Jiang M.H., *J. Chin. Phys. Lett.*, 13 (1986), 841.
[3] Iwai M., Kobayashi T., Furya H., Mori Y., Sasaki T., *Jpn. J. Appl. Phys.,* 36 (1997), L276.
[4] Ramamurthy N., Dhanuskodi S., Manjusha M.V., *J. Philip. Opt. Mater.,* 33 (4) (2011), 612.
[5] Venkatesan G., Anandha Babu G., Ramasamy P., Chandramohan A., *J. Mol. Struct.,* 121 (2013), 1033.
[6] Munn R.W., Ironside C.N., *Principles and Applications of Nonlinear Optical Materials,* Chapman & Hall, London, 1993.
[7] Jose M., Uthrakumar R., Jeya Rajendran A., Dass J., *Spectrochim. Acta A*, 86 (2012), 495.
[8] Lin L., Li J., Chen Y., *J. Cryst. Growth*, 249 (2003), 341.
[9] Alfred Cecil Rajs., Sinthiy A., Babu V., *Acta Crystallogr. E,* 68 (2012), 21825.
[10] Tanaka M., Matsuoka M., *J. Cryst. Growth*, 99 (1990), 1133.
[11] Silverstein R.M., Webster F.X., Kemal D.J., *Spectrometric Identification of Organic Compounds*, John Wiley & Sons Inc, 2005.
[12] Bridget Mary M., Sasirekha V., Ramakrishan V., *Spectrochim. Acta A*, 65 (2006), 420.
[13] Charles J.B., Gnanam F.D., *J. Mater. Sci. Lett.*, 12 (1993), 1397.

[14] MAYER M.A., LAERK VAN J.B., *Nature*, 164 (1947), 1129.
[15] ONITSCH M., *Mikroskopie*, 2 (1947), 151.
[16] THUL P., GUPTAV P., RAM V.J., TANDON P., *Spectrochim. Acta A*, 75 (2010), 260.
[17] POLITZER P., MURRAYJ S., BEVERIDGED L., LAVERY R., *Theoretical Biochemistry and Molecular Biophysics: A Comprehensive Survey*, Adenine Press, New York, 1991.
[18] MURRAYJ S., POLITZER P., *Croat. Chem. Acta*, 82 (1) (2009), 275.
[19] SZAFRAN M., KOMASA A., ADAMSKA E.B., *J. Mol. Struct.*, 827 (2007), 107.
[20] JAMES C., AMAL RAJ A., REGHUNATHAN R., JOE I.H., JAYAKUMAR V.S., *J. Raman Spectrosc.*, 37 (2006), 1392.
[21] LIUJ N., CHENZ R., YUANS F., ZHEJIAN G., *J. U. Sci. Tech. Beijing*, 6 (2005), 589.
[22] PARTHASARATHI R., PADMANABHAN J., SUBRAMANIANV V., SARKAR U., MAITI B., CHATTRAJ P.K., *Int. El. J. Mol. Des.*, 2 (2003), 813.
[23] KURTZ S.K., PERRY T.T., *J. Appl. Phys.*, 39 (1968), 3813.

Received 2017-04-01
Accepted 2018-01-24